Wideband dynamic numerical model of a tapered buried ridge stripe semiconductor optical amplifier gate

M.J. Connelly

Abstract: A wideband dynamic numerical model of a tapered buried ridge stripe semiconductor optical amplifier is described. The model is based on a carrier density rate equation and a set of travelling-wave equations describing the amplified signal fields and spontaneous emission photon rates. These equations are solved in time and space using a computationally efficient numerical algorithm. The model is used to predict the switching properties of an optical gate. A simple equivalent circuit model of the gate, including package parasitics, is derived that can be used in conventional electrical circuit simulation tools.

1 Introduction

Semiconductor optical amplifier (SOA) technology has matured to the point where commercial devices are available for use in optical communication systems. In optical fibre communication systems efficient use of the fibre bandwidth can be achieved using wavelength division multiplexing (WDM). These systems require wideband optical amplifiers. Optical communication systems are also operating at increasingly high bitrates. To model the effects that optical amplification using SOAs has on high-speed signals requires wideband dynamic models. Dynamic models are also required to model SOA applications such as switches and modulators. Many such models have been presented in the literature [1–4]. Most of these models use very simple analytical expressions for the amplifier material gain, which are only applicable for wavelengths near the gain peak. Most amplifier models also use a heuristic factor to estimate the amount of spontaneous emission generated in the amplifier. This factor is assumed to be constant. In actual fact the spontaneous emission added to travelling-waves in the amplifier is directly related to the amplifier gain, which is wavelength dependent. Most dynamic models also ignore the relationship between the radiative recombination lifetime and the material gain coefficient. This leads to inaccuracies between the model predictions and experimental results. The above limitations mean that most conventional models are only applicable over a narrow range of the amplifier bandwidth and operating conditions.

In this paper we present a wideband dynamic model and a numerically efficient algorithm. The dynamic model is based on the steady-state model developed in [5]. The model is then used to analyse the performance of an SOA gate. The particular amplifier considered in the model is a tapered homogeneous buried ridge stripe SOA with a bulk active region [6]. In addition a simple equivalent circuit model of the SOA is derived. This circuit model can be used to aid the design of the gate drive circuits, connecting transmission lines and impedance matching networks if required.

2 Amplifier structure and material model

A schematic diagram of the SOA under consideration is shown in Fig. 1. The device operates in the 1.55 μm region. The device structure consists of a central active region of width W, thickness d and length L_c. The active region narrows as a lateral taper of width W at the central active region to zero width at each end. The length of an individual taper is L_t. In the model it is assumed that the tapers linearly reduce the optical confinement factor from its maximum value of Γ_c in the central active region to zero at the amplifier ends. The function of the tapers is to improve the coupling efficiency to and from the amplifier. Buried windows are used at either end of the device to reduce the effective facet reflectivity. Geometrical and material parameters for the device under consideration are given in Table 1.

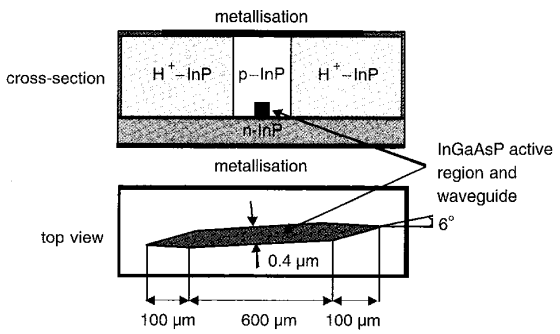

Fig. 1 *Cross-section and active region top view of a homogeneous buried ridge stripe SOA with tapered waveguides and buried windows*
The H^+ implanted InP aids carrier confinement

IEE Proceedings online no. 20020323

DOI: 10.1049/ip-cds:20020323

Paper first received 14th May and in revised form 16th November 2001

The author is with the Department of Electronic and Computer Engineering, University of Limerick, Limerick, Ireland

Table 1: SOA geometrical and model parameters

Symbol	Parameter	Value
L_c	Central active region length	600 μm
L_t	Taper length	100 μm
d	Active region thickness	0.4 μm
W	Central active region width	0.4 μm
Γ_c	Optical confinement factor of the central active region	0.45
E_{g0}	Bandgap energy at zero injected carrier density	0.774 eV
K_g	Bandgap shrinkage coefficient	1.4×10^{-10} eVm
m_e	Effective mass of electron in the CB	4.10×10^{-32} kg
m_{hh}	Effective mass of a heavy hole in the VB	4.19×10^{-31} kg
m_{hl}	Effective mass of a light hole in the VB	5.06×10^{-32} kg
η_{in}	Input coupling loss	2.5 dB
η_{out}	Output coupling loss	2.5 dB
R_1	Input facet reflectivity	5.0×10^{-5}
R_2	Output facet reflectivity	5.0×10^{-5}
K_o	Carrier-independent absorption loss coefficient, mainly caused by waveguide imperfections	10000 m^{-1}
K_1	Carrier-dependent absorption loss coefficient	2.0×10^{-20} m^2
B_{rad}	Bimolecular radiative recombination coefficient	6.8×10^{-16} m^3s^{-1}
A_{nrad}	Linear nonradiative recombination coefficient	0.0 s^{-1}
C_{aug}	Auger recombination coefficient	3.0×10^{-41} m^6s^{-1}

The material gain coefficient of the InGaAsP active region can be expressed as [5]

$$g_m(v,n) = \frac{c^2}{4\sqrt{2}\pi^{3/2} n_r^2 \tau v^2}\left[\frac{2m_e m_{hh}}{\hbar(m_e+m_{hh})}\right]^{3/2} \sqrt{v - \frac{E_g(n)}{h}}[f_c(v) - f_v(v)] \quad (1)$$

where c is the speed of light in a vacuum, v optical frequency, n_r the active region refractive index, τ the radiative carrier recombination lifetime and $\hbar$ Planck's constant h divided by 2π. m_e and m_{hh} are the conduction band (CB) electron and valence band (VB) heavy hole effective masses, respectively. n is the CB carrier (electron) density. The bandgap energy E_g can be expressed as

$$E_g(n) = E_{g0} - eK_g n^{1/3} \quad (2)$$

where K_g is the bandgap shrinkage coefficient [7]. The Fermi–Dirac distributions in the CB and VB are given by

$$f_c(v) = \left[\exp\left(\frac{E_a - E_{fc}}{kT}\right) + 1\right]^{-1}$$
$$f_v(v) = \left[\exp\left(\frac{E_b - E_{fv}}{kT}\right) + 1\right]^{-1} \quad (3)$$

with

$$E_a = [hv - E_g(n)]\frac{m_{hh}}{m_e + m_{hh}}$$
$$E_b = -[hv - E_g(n)]\frac{m_e}{m_e + m_{hh}} \quad (4)$$

T is absolute temperature and k the Boltzmann constant. The quasi-Fermi levels E_{fc} in the CB and E_{fv} in the VB can be estimated using the Nilsson approximation [8],

$$E_{fc} = \left\{\ln\delta + \delta\left[64 + 0.05524\,\delta\left(64 + \sqrt{\delta}\right)\right]^{-\frac{1}{4}}\right\} kT$$
$$E_{fv} = -\left\{\ln\varepsilon + \varepsilon\left[64 + 0.05524\,\varepsilon\left(64 + \sqrt{\varepsilon}\right)\right]^{-\frac{1}{4}}\right\} kT \quad (5)$$

where

$$\delta = \frac{n}{n_c};\ \varepsilon = \frac{p}{n_v} \quad (6)$$

p is the VB hole density. At the carrier density levels usually present in SOAs p is equal to n. n_c and n_v are constants given by

$$n_c = 2\left(\frac{m_e kT}{2\pi\hbar^2}\right)^{\frac{3}{2}};\ n_v = 2\left(\frac{m_{dh} kT}{2\pi\hbar^2}\right)^{\frac{3}{2}} \quad (7)$$

where

$$m_{dh} = \left(m_{hh}^{\frac{3}{2}} + m_{lh}^{\frac{3}{2}}\right)^{\frac{2}{3}} \quad (8)$$

m_{lh} is the effective mass of a light hole in the VB. $\Gamma(z)$ is the optical confinement factor modelled by

$$\Gamma(z) = \begin{cases} \Gamma_c \frac{z}{L_t} & ;0 \le z < L_t \\ \Gamma_c & ;L_t \le z \le L_t + L_c \\ \Gamma_c\left(\frac{2L_t + L_c - z}{L_t}\right) & ;L_t + L_c < z \le 2L_t + L_c \end{cases} \quad (9)$$

where z lies along the amplifier axis with its origin at the input facet.

3 Travelling-wave equations for the signal field

In the model, the input signal has optical frequency v_s and power $P_{s,in}$ before coupling loss. The signal travels through the amplifier, aided by the embedded waveguide, and exits at the opposite facet. The SOA model is based on a set of coupled differential equations that describe the interaction between the carrier density and photon rates. In the model the left (input) and right (output) facets have power reflectivities R_1 and R_2, respectively. Within the amplifier the spatially varying component of the signal field can be decomposed into two complex travelling-waves, E_s^+ and E_s^-, propagating in the positive and negative z-directions, respectively. The modulus squared of the amplitude of a travelling-wave is taken to be equal to the photon rate (s^{-1}) of the wave in that direction, so

$$N_s^+ = |E_s^+|^2;\ N_s^- = |E_s^-|^2 \quad (10)$$

In the model it is assumed that the temporal properties of the input optical signals and driving current are on a time scale much greater than the amplifier transit time τ_{tr}, given by

$$\tau_{tr} = \frac{(L_c + 2L_t)n_r}{2c} \quad (11)$$

Typical values of the transit time are of the order of picoseconds. Most conventional optical modulation schemes have time scales much greater than τ_{tr}. Furthermore it can be assumed that the light intensity responds instantaneously to temporal changes in the carrier density. In this case E_s^+ and E_s^- can be modelled by the travelling-wave equations [5],

$$\frac{dE_s^{\pm}(z,t)}{dz} = \pm\left\{-j\beta + \frac{1}{2}[\Gamma(z)g_m(v_s,n) - \alpha(n)]\right\}E_s^{\pm}(z,t) \tag{12}$$

where $j = \sqrt{-1}$ and the signal propagation coefficient is

$$\beta = \frac{2\pi n_{eq} v_s}{c} \tag{13}$$

where n_{eq} is the equivalent index of the amplifier waveguide [9]. The material loss coefficient α is modelled as a linear function of carrier density [9]

$$\alpha(n) = K_0 + \Gamma(z)K_1 n \tag{14}$$

The boundary conditions of (12) are

$$E_s^+(0,t) = (1 - \sqrt{R_1})E_{s,in}(t) + \sqrt{R_1}\,E_s^-(0,t)$$

$$E_s^-(L,t) = \sqrt{R_2}E_s^+(L,t) \tag{15}$$

where R_1 and R_2 are the facet reflectivities. The input signal field is

$$E_{s,in}(t) = \sqrt{\frac{\eta_{in}P_{s,in}(t)}{hv_s}} \tag{16}$$

The output signal power after coupling loss is

$$P_{s,out}(t) = hv_s\eta_{out}R_2\left|E_s^+(L,t)\right|^2 \tag{17}$$

η_{in} and η_{out} are the input and output coupling efficiencies, respectively.

4 Travelling-wave equations for the spontaneous emission

The amplification of the signal also depends on the amount of spontaneously emitted noise generated by the amplifier. This is because the noise power takes part in draining the available carrier population and helps saturate the gain. It is not necessary to treat the spontaneous emission as a coherent signal since it distributes itself continuously over a relatively wide band of wavelengths with random phases between adjacent wavelength components. When reflecting facets are present the spontaneously emitted noise will show the presence of longitudinal cavity modes. For this reason it may be assumed that noise photons only exist at discrete frequencies corresponding to integer multiples of cavity resonances. These frequencies are given by

$$v_k = v_c + \Delta v_c + kK_m\Delta v_m \;; k = 0 \ldots N_m - 1 \tag{18}$$

$v_c = E_{g0}/h$ is the cutoff frequency at zero injected carrier density. Δv_c is a frequency offset used to match v_0 to a resonance. K_m and N_m are positive integers. The values of K_m and N_m chosen depend on the gain bandwidth of the SOA and accuracy required from the numerical solution of the model equations. This technique greatly reduces computation time. In the numerical simulations described below $K_m = 20$ and $N_m = 40$. The longitudinal mode frequency spacing is

$$\Delta v_m = \frac{c}{2\int_0^L n_{eq}dz} \tag{19}$$

The detailed shape of the noise output can then be determined using the method given in [5]. N_k^+ and N_k^- are defined as the spontaneous emission photon rates (s^{-1}) for a particular polarisation in a frequency spacing $K_m\Delta v_m$ centred on frequency v_k, travelling in the positive and negative z directions, respectively. N_k^+ and N_k^- obey the travelling-wave equations [5]

$$\frac{dN_k^{\pm}(z,t)}{dz} = \pm[\Gamma(z)g_m(v_k,n) - \alpha(n)]N_k^{\pm}(z,t) \pm R_{sp}(v_k,n) \tag{20}$$

subject to the boundary conditions

$$N_k^+(0,t) = R_1 N_k^-(0,t)$$

$$N_k^-(L,t) = R_2 N_k^+(L,t) \tag{21}$$

R_{sp} is given by

$$R_s(v_k,n) = \Gamma(z)g'_m(v_k,n)K_m\,\Delta v_m \tag{22}$$

with

$$g'_m = \frac{c^2}{4\sqrt{2}\pi^{3/2}n_r^2\tau v^2}\left[\frac{2m_e m_{hh}}{\hbar(m_e + m_{hh})}\right]^{3/2} \sqrt{v - \frac{E_g(n)}{h}}\,f_c(v)\,[1 - f_v(v)] \tag{23}$$

The amplifier finite facet reflectivities cause filtering of the spontaneous noise. To account for this N_k^+ and N_k^- are multiplied by a normalisation factor T_K given by

$$T_k = \frac{1}{\sqrt{1+\gamma^2}} \tag{24}$$

where

$$\gamma = \frac{4G_s(v_k)\sqrt{R_1R_2}}{\left[1 - \sqrt{R_1R_2}G_S(v_k)\right]^2} \tag{25}$$

T_k is equal to unity for zero facet reflectivities.

5 Carrier density rate equation

The carrier density at z obeys the rate equation

$$\frac{dn(z,t)}{dt} =$$

$$\frac{I(t)}{ed(L_c + L_t)W} - R(n) - \frac{\Gamma(z)}{dW}g_m(v_s,n)[N_s^+(z,t) + N_s^-(z,t)]$$

$$-\frac{2\Gamma(z)}{dW}\left\{\sum_{k=0}^{N_m-1} g_m(v_k,n)T_k\left[N_k^+(z,t) + N_k^-(z,t)\right]\right\} \tag{26}$$

where $I(t)$ is the current injected into the active region. The recombination rate term $R(n)$ is given by

$$R(n) = A_{nrad}n + B_{rad}n^2 + C_{aug}n^3 \tag{27}$$

In (27), A_{nrad} and B_{rad} are the linear nonradiative and bimolecular radiative recombination coefficients, respectively. C_{aug} is the Auger nonradiative recombination coefficient. The radiative recombination lifetime can be approximated by

$$\tau = \frac{1}{B_{rad} n} \tag{28}$$

In the model the amplifier is assumed to be polarisation independent. Polarisation dependence can be included by the use of different optical confinement factors for the amplifier transverse electric and transverse magnetic modes. In the amplifier modelled the experimental polarisation sensitivity was 0.12 dB so the polarisation insensitive model is well justified.

6 Dynamic numerical algorithm

As the SOA model equations cannot be solved analytically, a numerical solution is required. A flow chart of the dynamic numerical algorithm is shown in Fig. 2. The first step in the algorithm is to initialise the signal fields and spontaneous emission photon rates using the steady-state algorithm described in [5]. The time iteration now begins. The coefficients of the travelling-wave equations are computed. Next the signal fields and noise photon densities are estimated using finite difference solutions of (12) and (20). In the finite difference solution the amplifier is split into a number of sections. The larger the number of sections used in the model, the greater the accuracy but the longer the simulation run time. For the particular SOA modelled it was found that using more than 20 sections gave a minimal increase (< 1%) in simulation accuracy. The signal fields and spontaneous emission photon rates are estimated at the section interfaces. In evaluating the right-hand side of (26), Q for the ith section, the signal and noise photon rates used are given by the mean value of those quantities at the section boundaries. After the noise has been normalised, the amplifier output parameters such as fibre-to-fibre gain, noise figure and noise power spectrum are calculated. If the simulation time limit is reached the algorithm stops. The choice of time step Δt is of paramount importance for good stability. For relatively slow input optical signals and current, the dynamic performance of the amplifier is to a large degree determined by the carrier lifetime. The carrier lifetime is of the same order as τ. In this case to avoid erratic simulation results the ratio of Δt to τ should be of the order of 10%. For amplifier inputs with time-varying behaviour faster than τ, Δt should be a fraction of the fastest input time scale.

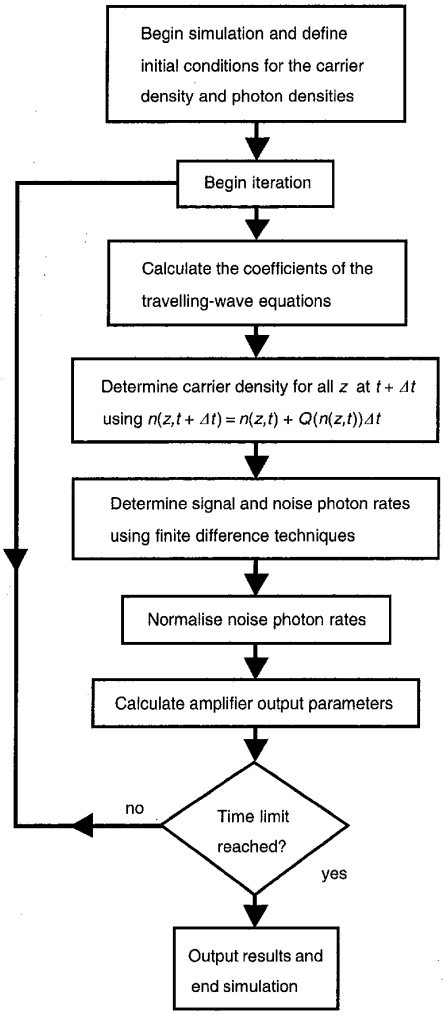

Fig. 2 *SOA dynamic model numerical algorithm*

7 Optical gate simulations

As SOAs have wide gain bandwidths and short carrier lifetimes they can be used as high-speed optical gates in WDM networks. In the European Union HARMONICS (Hybrid Access Reconfigurable Multiwavelength Optical Networks for IP-based Communication Services) project there is a requirement for such an optical gate. The gate specifications required are listed in Table 2. Dynamic simulations can be used to predict if these specifications can be met for a given device structure and material. The device material parameters used in the dynamic model were obtained by matching steady-state simulations and experimental data as shown in Fig. 3. Using the dynamic algorithm described above, the intrinsic (i.e. not considering device structural and package parasitics) switching performance of the device can be analysed. The first specification that needs to be met is the fibre-to-fibre gain of 10 dB for a peak input power of −7 dBm at a maximum drive current of 60 mA in the on state. The predicted gain for this condition is 7 dB, which is 3 dB less than that specified. Static simulations indicate that the gain requirement can be met with a total device length of 700 μm, including 100 μm long tapers. The predicted gain against bias characteristic, shown in Fig. 4, can be used to choose the SOA gate off current. The model parameters also show that the K_0 coefficient is relatively large compared to values in a higher-gain device with an identical structure [5]. This loss coefficient is primarily due to waveguide losses, probably caused by irregularities in the waveguide thickness and

Table 2: SOA gate requirements

Operating temperature	300 K
Wavelength	1554 nm
Fibre-to-fibre gain at −7 dBm input power	10 dB
Maximum drive current	60 mA
On-off ratio	> 60 dB
Rise and fall times	< 10 ns

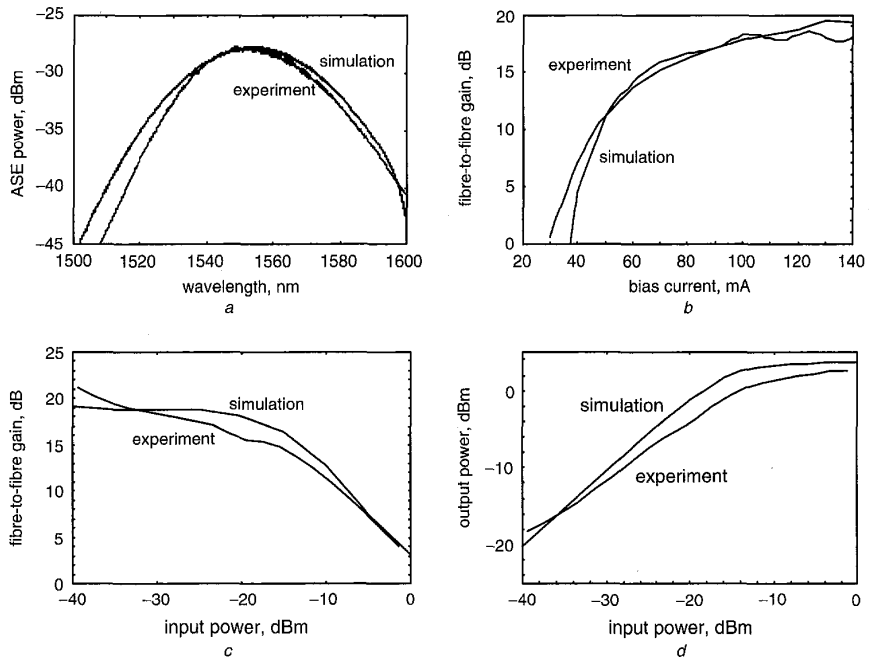

Fig. 3 *Comparisons between experiment and steady-state simulation, used to obtain the device modelling parameters*
Signal wavelength is 1554 nm
a SOA output ASE spectrum with a resolution bandwidth of 0.7 nm, bias current = 120 mA, input power = −30 dBm
b Fibre-to-fibre gain versus bias current, $P_{in} = -30$ dBm
c Fibre-to-fibre gain against input optical power, bias = 120 mn
d Output signal power input power, bias = 120 mA

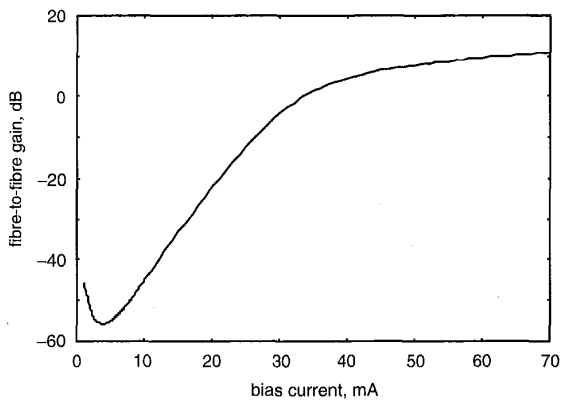

Fig. 4 *Predicted gain against bias current characteristic for a 700 μm long SOA*
Input power = −7 dBm; wavelength = 1554 nm

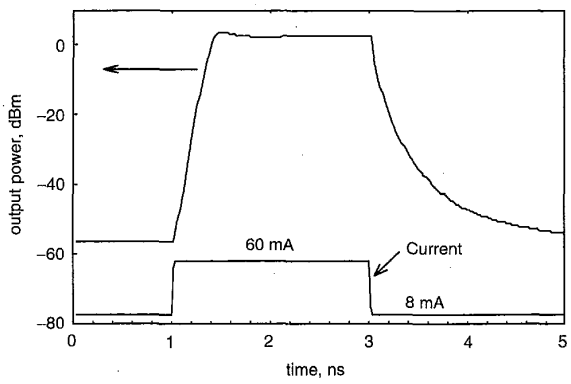

Fig. 5 *SOA gate switching characteristic*
Input signal power = −7 dBm; wavelength = 1554 nm
In this case both the rise and fall times are equal to 0.18 ns. The rising edge of the switched optical signal is faster than the falling edge. This is because the carrier density increases as the gate is switched on leading to a relatively short carrier lifetime. Conversely as the gate is switched off the carrier density decreases leading to a longer carrier lifetime

width. These losses can be reduced through improvements in the device fabrication process. It is advantageous to choose the smallest possible on and off currents, as this makes the current drive circuit speed requirements easier to satisfy. Using on and off currents of 8 mA and 60 mA, respectively give an optical on–off ratio of 60 dB at an input power of −7 dBm. The dynamic model can now be used to determine if the switching speed requirements of the gate can be met. The predicted gate switching characteristic is shown in Fig. 5. The gate rise time τ_r is defined as the time taken for the output signal power to rise from 20 dB below its static value in the on state to its final on-state value when the gate is switched on. Conversely, the fall time τ_f is defined as the time taken for the output signal power to fall by 20 dB below its on-state value when the gate is switched off. From Fig. 5, the rise and fall time are both equal to 0.18 ns comfortably less than the value of 10 ns required.

8 Intrinsic SOA gate equivalent circuit model

The active region of the SOA is a forward-biased *p–n* junction. From an electrical perspective, it can be modelled as a series resistance R_s caused by the resistivity of the active

region material and a parallel combination of the junction capacitance C_j and junction resistance R_j. These can be approximated by

$$R_j = \frac{dV_j}{dI_j}$$
$$C_j = -ed(L_c + L_t)W\frac{dn_j}{dV_j} \quad (29)$$

where V_j and I_j are the average junction voltage (equal to the quasi-Fermi level difference) and current, respectively, and n_j the average active region carrier density. The values of R_j and C_j can be obtained from the static model. R_s is small and can be neglected in the analysis. For a current range of 5–60 mA the average values of C_j and R_j are approximately 0.2 nF and 0.5 Ω, respectively. The device structural parasitics such as the InP homojunction capacitance have negligible effects on the gate performance [10].

9 Package parasitics

External connections to the SOA will contribute extra parasitics that can limit the gate speed. These parasitics can be modelled as a parallel capacitance C_p (due to the bond pad) and a series inductance L_p (due to the bond wire inductance). The equivalent circuit model shown in Fig. 6 can be used to represent the SOA chip and package parasitics. R_m is the resistance of the cladding regions, which can be determined by modelling the cladding regions of the amplifier by resistive ladder networks and using an electrical circuit simulation tool. Using this technique for the particular SOA under consideration a value of 2.5 Ω was found for R_m. From the circuit model, the ratio of the current phasor $I_{SOA}(j\omega)$ flowing through the SOA to the total input current phasor $I_{in}(j\omega)$, in the case where $\omega C_j R_j << 1$, is

$$\frac{I_{SOA}(j\omega)}{I_{in}(j\omega)} = \frac{1}{(1 - L_p C_p \omega^2) + j\omega(R_m + R_j)C_p} \quad (30)$$

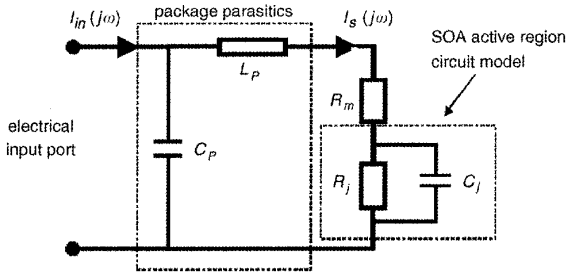

Fig. 6 *SOA circuit model including package parasitics*

where ω is the angular frequency. Equation (30) can be used to plot contours of constant 3-dB bandwidth (f_{3dB}) for a particular value of $R_m + R_j$. The rise and fall time of the circuit model are approximately equal to $0.35/f_{3dB}$. An example set of contours is shown in Fig. 7, from which the maximum allowable values of the package parasitics for a given 3-dB bandwidth can be determined. If the circuit rise and fall times are less than the required switching time, the SOA gate dynamic performance will be satisfactory.

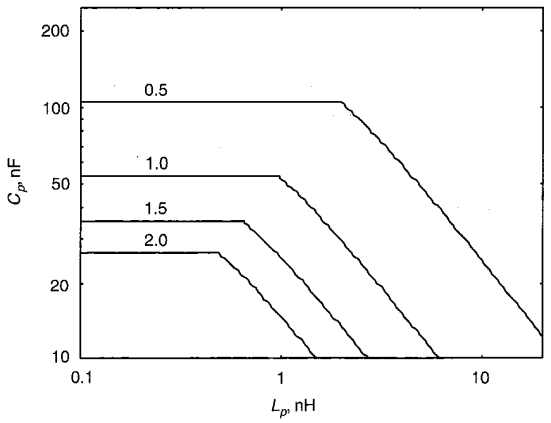

Fig. 7 *SOA circuit model 3-dB frequency contours*
The parameter is the 3-dB frequency in GHz. The intrinsic SOA switching speed is assumed to be much greater than the 3-dB frequency. In this case the intrinsic SOA is modelled as a resistance $R_{SOA} = R_m + R_j = 3.0\,\Omega$

10 Conclusions

A comprehensive physical model of an SOA gate has been developed, from which a simple circuit model was obtained. The model can be used to predict the gate switching performance. The external limitation to achieving the intrinsic switching speed is caused by package parasitics. 3-dB frequency contours were calculated that allow the maximum package parasitics allowable to be estimated.

11 Acknowledgment

This work was supported in part by the European Union under the IST HARMONICS project.

12 References

1 DURHUUS, T., MIKKELSEN, B., and STUBKJAER, K.E.: 'Detailed dynamic model for semiconductor optical amplifiers and their crosstalk and intermodulation distortion', *J. Lightwave Technol.*, 1992, **10**, (8), pp. 1056–1065
2 WONG, W.M., and GHAFOURI-SHIRAZ, H.: 'Dynamic model of tapered semiconductor lasers and amplifiers based on transmission-line laser modeling', *IEEE J. Sel. Top. Quantum Electron.*, 2000, **6**, (4), pp. 585–593
3 GUTIERREZ-CASTREJON, R., SCHARES, L., OCCHI, L., and GUEKOS, G.: 'Modeling and measurement of longitudinal gain dynamics in saturated semiconductor optical amplifiers of different length', *IEEE J. Quantum Electron.*, 2000, **26**, (12), pp. 1476–1484
4 TOPTCHIYSKI, G., KINDT, S., PETERMANN, K., HILLIGER, E., DIEZ, S., and WEBER, H.G.: 'Time-domain modeling of semiconductor optical amplifiers for OTDM applications', *J. Lightwave Technol.*, 1999, **17**, (12), pp. 2577–2583
5 CONNELLY, M.J.: 'Wideband semiconductor optical amplifier steady-state numerical model', *IEEE J. Quantum Electron.*, 2001, **37**, (3), pp. 439–447
6 DEGUET, C., DELPRAT, D., CROUZEL, G., TRAYNOR, N.J., MAIGNE, P., PEARSAL, T., LERMINIAUX, C., ANDREAKIS, N., CANEAU, C., FAVIRE, F., BHAT, R., and ZAH, C.E.: 'Homogeneous buried ridge stripe semiconductor optical amplifier with near polarisation independence'. Proceedings of the European Conference on Optical Communications, 1999
7 ADACHI, S.: 'GaAs and related materials' (World Scientific Publishing, 1994)
8 NILSSON, N.G.: 'Empirical approximations for the Fermi energy of a semiconductor with parabolic bands', *Appl. Phys. Lett.*, 1978, **33**, pp. 653–654
9 SUEMMATSU, Y., and ADAMS, A.R.: 'Handbook of semiconductor lasers and photonic integrated circuits' (Chapman and Hall, London, 1994)
10 AMANN, M.-C., and THULKE, W.: 'Current confinement and leakage currents in planar buried-ridge-structure laser diodes on n-substrate', *IEEE J. Quantum Electron.*, 1989, **25**, pp. 1595–1602